

## Article

# Hybrid Polyelectrolyte Capsules Loaded with Gadolinium-Doped Cerium Oxide Nanoparticles as a Biocompatible MRI Agent for Theranostic Applications

Danil D. Kolmanovich <sup>1</sup>, Nikita N. Chukavin <sup>1</sup> , Irina V. Savintseva <sup>1</sup>, Elena A. Mysina <sup>1</sup>, Nelli R. Popova <sup>1</sup>, Alexander E. Baranchikov <sup>2,\*</sup> , Madina M. Sozarukova <sup>2</sup> , Vladimir K. Ivanov <sup>2</sup>  and Anton L. Popov <sup>1,\*</sup> 

<sup>1</sup> Institute of Theoretical and Experimental Biophysics, Russian Academy of Sciences, Pushchino 142290, Russia

<sup>2</sup> Kurnakov Institute of General and Inorganic Chemistry, Russian Academy of Sciences, Moscow 119991, Russia

\* Correspondence: a.baranchikov@yandex.ru (A.E.B.); antonpopovleonid@gmail.com (A.L.P.)

**Abstract:** Layer-by-layer (LbL) self-assembled polyelectrolyte capsules have demonstrated their unique advantages and capability in drug delivery applications. These ordered micro/nanostructures are also promising candidates as imaging contrast agents for diagnostic and theranostic applications. Magnetic resonance imaging (MRI), one of the most powerful clinical imaging modalities, is moving forward to the molecular imaging field and requires advanced imaging probes. This paper reports on a new design of MRI-visible LbL capsules, loaded with redox-active gadolinium-doped cerium oxide nanoparticles (CeGdO<sub>2-x</sub> NPs). CeGdO<sub>2-x</sub> NPs possess an ultrasmall size, high colloidal stability, and pronounced antioxidant properties. A comprehensive analysis of LbL capsules by TEM, SEM, LCSM, and EDX techniques was carried out. The research demonstrated a high level of biocompatibility and cellular uptake efficiency of CeGdO<sub>2-x</sub>-loaded capsules by cancer (human osteosarcoma and adenocarcinoma) cells and normal (human mesenchymal stem) cells. The LbL-based delivery platform can also be used for other imaging modalities and theranostic applications.

**Keywords:** cerium oxide nanoparticles; gadolinium; polyelectrolyte microcapsules; MRI agent



**Citation:** Kolmanovich, D.D.; Chukavin, N.N.; Savintseva, I.V.; Mysina, E.A.; Popova, N.R.; Baranchikov, A.E.; Sozarukova, M.M.; Ivanov, V.K.; Popov, A.L. Hybrid Polyelectrolyte Capsules Loaded with Gadolinium-Doped Cerium Oxide Nanoparticles as a Biocompatible MRI Agent for Theranostic Applications. *Polymers* **2023**, *15*, 3840. <https://doi.org/10.3390/polym15183840>

Academic Editors: Anatoly Olkhov and Polina Tyubaeva

Received: 22 August 2023

Revised: 19 September 2023

Accepted: 19 September 2023

Published: 21 September 2023



**Copyright:** © 2023 by the authors. Licensee MDPI, Basel, Switzerland. This article is an open access article distributed under the terms and conditions of the Creative Commons Attribution (CC BY) license (<https://creativecommons.org/licenses/by/4.0/>).

## 1. Introduction

Medical imaging has long served as an important tool for diagnosis and therapeutic efficacy monitoring. MRI is safe and has a very high spatial resolution of around 25–100  $\mu\text{m}$  in different magnetic fields. Today, gadolinium-containing compounds are widely used as MRI contrast agents [1]. The Gd<sup>3+</sup> ion has seven unpaired electrons ( $8S^{7/2}$ ) and an exceptionally high magnetic moment (7.94 BM), which enables the use of gadolinium-containing compounds as contrast agents in magnetic resonance imaging (MRI). Gadolinium in ionic form is very toxic and can potentially cause nephrogenic systemic fibrosis (NSF) [2,3]. In this regard, various chelating compounds are used, for example, dipyradoxal phosphate, 1,4,7,10-tetraazacyclododecane-1,4,7,10-tetraacetic acid, diethylenetriaminepentaacetic acid, etc., which limit its direct contact with biological fluids. This principle is implemented in all known clinical preparations based on gadolinium (Omniscan<sup>®</sup>, OptiMark<sup>®</sup>, MultiHance<sup>®</sup>, Primovist<sup>®</sup>, and Vasovist<sup>®</sup>). At the same time, poorly soluble gadolinium oxide is a more stable compound than its ionic form and does not have toxic effects either in vitro or in vivo [4,5]. Gadolinium oxide in nanocrystalline form is considered one of the most promising contrast agents for MRI, due to its higher value of longitudinal relaxation constants in comparison with Gd<sup>3+</sup> chelate complexes [6].

The cerium oxide nanoparticle (nanoceria, CeO<sub>2</sub>) is the most promising inorganic nanozyme, and it is used in various areas of biomedicine. It has strong antioxidant [7], radioprotective [8], and anti-inflammatory properties [9]. At the same time, the doping of cerium oxide with Gd<sup>3+</sup> ions increases its oxygen nonstoichiometry and, consequently,

enhances the antioxidant activity of the nanoparticles [10], and also increases T1 relaxivity. Thus, gadolinium-doped cerium oxide nanoparticles are a good ground for the design of new theranostic agents, which possess both high redox activity and MRI contrasting ability.

It has been shown recently that nanoceria is capable of exhibiting selective cytotoxicity against cancer cells [11–13], but the ultrasmall particle size of bioactive nanoceria and its high reactivity limits the effective targeted delivery to tissues and organs. In this regard, there is a need to create advanced nanoceria delivery systems providing the concentration and delivery time control. One possible solution to this problem is the use of polyelectrolyte microcapsules. Polyelectrolyte capsules are constructed through layer-by-layer (LbL) self-assembly techniques and have been shown to be a promising platform for various biomedical applications [14–20]. The advantages of LbL capsules include the ease of their size, chemical control, and the design of their structure, the wide variety of self-assembling polyelectrolytes [16,21], the mild loading environment, and controlled permeability. Polyelectrolyte capsules have been used for the controlled encapsulation and release of small molecule drugs [22], enzymes [23], protein drugs [24], DNA [25], etc.

In this work, LbL polyelectrolyte capsules made from biodegradable polymers were used as an intracellular delivery system for gadolinium-doped cerium oxide nanoparticles. The research entailed the synthesis of polyelectrolyte microcapsules modified with redox-active  $\text{CeGdO}_{2-x}$  NPs, a comprehensive analysis of their physicochemical properties and biocompatibility, and the demonstration of their ability to act as an MRI contrast agent.

## 2. Materials and Methods

### 2.1. Materials

Calcium chloride ( $\text{CaCl}_2$ , #223506), sodium carbonate ( $\text{Na}_2\text{CO}_3$ , #S7795), ethylenediaminetetraacetic acid disodium salt dihydrate ( $\text{Na}_2\text{EDTA}$ , #E5134), citric acid ( $\text{HOC}(\text{COOH})(\text{CH}_2\text{COOH})_2$ , #C0759), cerium (III) chloride heptahydrate ( $\text{CeCl}_3 \cdot 7\text{H}_2\text{O}$ , #22300), gadolinium(III) nitrate hexahydrate (#451134), dextran sulfate sodium salt (DS, MW  $\approx$  10 kDa, #D4911), 4-iodophenol (#I10201), and poly-L-arginine hydrochloride (PArg, MW  $\approx$  70 kDa, #P3892), were purchased from Sigma-Aldrich. All chemicals were used as received. Ultrapure water with a resistance greater than  $18.2 \text{ M}\Omega \text{ cm}^{-1}$  was used for all experiments. MTT reagent and Hoechst 33,342 dye were purchased from PanEKO (Moscow, Russia). A live/dead assay kit, LDH assay kit, rhodamine B isothiocyanate, and phalloidin-FITC were purchased from Thermo Fisher Scientific, Cambridge, UK.

### 2.2. $\text{CeGdO}_{2-x}$ NPs Synthesis and Characterisation

An aqueous solution containing cerium (III) chloride and gadolinium (III) nitrate was prepared, with a total concentration of rare earth elements of 2 mM. The molar ratio of cerium to gadolinium was 4:1. An anion exchange resin in the OH form was added to the resulting solution until pH 10.0 was reached. The resulting solution was separated from the anion exchange resin by filtration and then subjected to hydrothermal treatment at  $150 \text{ }^\circ\text{C}$  for 1.5 h, after which it was cooled to room temperature. The sol was stabilised using sodium citrate (cerium/citrate molar ratio was 1:4). Then, the pH of the sol was adjusted to 7–8 by dropwise addition of aqueous ammonia.

The absorption spectra of the  $\text{CeGdO}_{2-x}$  NPs were measured on a Lambda 950 UV/VIS spectrometer (Perkin-Elmer, Shelton, CT, USA). TEM images were acquired using a JEOL-JEM 2010 transmission electron microscope (JEOL, Tokyo, Japan). EDX analysis was performed using an FEI Inspect F microscope. The hydrodynamic diameter and the zeta potential values were measured using a Zetasizer Nano ZS analyzer (Malvern Instruments Ltd., Malvern, UK). The aggregative stability of the  $\text{CeGdO}_{2-x}$  NPs was studied by dynamic light scattering 1 h after the formation of the  $\text{CeGdO}_{2-x}$  NPs' suspension in a phosphate buffer (pH 7.4) (PanEco, Moscow, Russia), DMEM/F12 culture medium (PanEco, Russia), and DMEM/F12 culture medium containing 10% fetal bovine serum (HyClone, Logan, UT, USA).

### 2.3. The Synthesis and Characterisation of the Capsules

Calcium carbonate ( $\text{CaCO}_3$ ) was used as a template. The  $\text{CaCO}_3$  synthesis was initiated by rapid mixing of equal volumes of  $\text{CaCl}_2$  and  $\text{Na}_2\text{CO}_3$  aqueous solutions at room temperature. After intensive stirring, with a magnetic stirrer for 30 s, the precipitate was separated by centrifugation at 1000 rpm for 1 min and washed three times with water. As a result, an aqueous suspension was formed containing spherical  $\text{CaCO}_3$  microparticles with an average diameter of 3 to 4  $\mu\text{m}$ . The first polyelectrolyte layer was deposited on the microparticles' surface by adsorption of positively charged poly-L-arginine hydrochloride (PARg) using a  $1 \text{ mg/mL}^{-1}$  PARg solution in 0.15 M NaCl (15 min incubation and shaking). The second layer was deposited by absorbing a negatively charged sodium dextran sulfate (DS) from a  $1 \text{ mg/mL}^{-1}$  DS solution in 0.15 M NaCl (15 min incubation and shaking). The core/polyelectrolyte particles were washed three times with deionised water after each adsorption step. A colloidal solution of  $\text{CeGdO}_{2-x}$  NPs was taken at a concentration of 0.5 mg/mL. The calcium carbonate nuclei were dissolved in ethylenediaminetetraacetic acid (EDTA) for 30 min, then centrifuged and washed three times with EDTA and then three times with water. The capsule consisted of a biodegradable polyelectrolyte PARg and DS with cerium gadolinium oxide nanoparticles in the middle layer (PARg/DS) (PARg/ $\text{CeGdO}_{2-x}$  NPs) (PARg/DS).

The absorption UV spectra of the  $\text{CeGdO}_{2-x}$  NPs-loaded capsules were measured on a Perkin-Elmer Lambda 950 UV/VIS spectrometer. TEM images were acquired using a JEOL-JEM 2010 transmission electron microscope. Scanning electron microscopy (SEM) and EDX analyses were performed using an FEI Inspect F microscope. Laser scanning confocal microscopy (LSCM) images were acquired using a Leica TS laser scanning confocal microscope with a  $63\times f/1.4$  oil immersion lens. Rhodamine B isothiocyanate (RBITC) labeled dextran was used as a fluorescent marker for the synthesis of the capsules and to study their intracellular localization.

### 2.4. Cell Culture

Cytotoxicity and cellular uptake analyses were carried out on three types of cell cultures: human osteosarcoma cells (MNNG/Hos), human adenocarcinoma cells (MCF-7), and human mesenchymal stem cells (hMSc) isolated from the dental pulp of a healthy orthodontics patient (with his written consent). All cells were deposited in the cryobank of the Theranostics and Nuclear Medicine Laboratory in ITEB RAS. Cells were cultured in a DMEM/F12 cultural medium containing 10% fetal calf serum (Cytiva, Shrewsbury, MA, USA) and a mixture of antibiotics (penicillin-streptomycin) (PanEco, Russia). The cells were cultured in 75  $\text{cm}^2$  flasks (SPL, Pocheon-si, Korea) in a  $\text{CO}_2$  incubator (RWD, Shenzhen, China).

### 2.5. MTT Assay

Cytotoxicity was assessed using a standard MTT assay [26]. Cells were seeded in 96 well plates (SPL, Korea) at a density of  $2.5 \times 10^4/\text{cm}^2$  in a DMEM/F12 culture medium (PanEko, Russia) containing 10% fetal calf serum (HyClone, Logan, UT, USA). After 8 h, capsules (1, 10, and 100 capsules per cell) were added to the cells. Then, after 24, 48, and 72 h, the medium was replaced with a solution of the MTT reagent (0.5 mg/mL). After 3 h of incubation with the MTT reagent, 100  $\mu\text{L}$  of DMSO (PanEko, Russia) was added. The optical density of the formazan solution in DMSO was determined using a BioRad plate reader 680 (BioRad, Ramsey, MN, USA) at 540 nm wavelength.

### 2.6. LDH Assay

Cells were seeded in 96-well plates and cultured in an atmosphere containing 5%  $\text{CO}_2$ , at 37  $^\circ\text{C}$ . Six hours after cell seeding, the medium was replaced with the similar medium containing 1, 10, or 100 capsules per cell. Triton X-100 was used as a positive control. Within 72 h after the addition of the  $\text{CeGdO}_{2-x}$  NP-loaded capsules, the level of lactate dehydrogenase in the culture medium was determined, according to the manufacturer's

protocol (The Thermo Scientific™ Pierce™ LDH Cytotoxicity Assay Kit, Cambridge, UK). Absorbance of the solution was measured at wavelengths of  $\lambda = 490$  nm and  $\lambda = 640$  nm, using the Microplate Reader ThermoMultiskan Ascent 96 & 384 (Thermo Fisher Scientific, Cambridge, UK).

### 2.7. Cellular Uptake

Rhodamine B isothiocyanate (RBITC)-labelled capsules were used for intracellular visualisation. The cells were seeded in 35 mm Petri dishes with a central hole (Ibidi, Fitchburg, WI, USA), at a density of  $2 \times 10^3$  per  $\text{cm}^2$ . After attachment and spreading of the cells (8 h), RBITC-labelled capsules were added (10 capsules per cell) and incubated with the cells for 16 h. After that, the cells were washed three times with Hank's solution and were stained to show actin cytoskeleton (phalloidin-FITC, Thermo Fisher Scientific, UK) and the cell nucleus (Hoechst 33342, PanEco, Russia). Micrographs were taken on a Zeiss Axiovert 200 (Zeiss, Jena, Germany) inverted microscope at a magnification of  $63\times$  with oil immersion.

### 2.8. MRI Scanning

MRI studies of  $\text{CeGdO}_{2-x}$ -loaded capsules were carried out using a Bruker Clinscan 7T MRI tomograph (Bruker, Billerica, MA, USA). For the measurements, the samples were diluted with an HEPES buffer solution to concentrations ranging from 0.1 mM to 1 mM, taking into account the efficiency of the loading of the nanoparticles and the concentration of nanoparticles per capsule. The SI dependencies on TI for each concentration were plotted and the T1 relaxation time was determined by the Mathcad approximation.  $1/T1$  ( $\text{s}^{-1}$ ) values were calculated from experimentally determined T1 relaxation times. T1 relaxivity values were calculated as the tangent of the inclination angle in the dependencies of the reverse T1 relaxation time on the  $\text{Gd}^{3+}$  concentration.

### 2.9. Antioxidant Activity of $\text{CeGdO}_{2-x}$ NPs

$\text{H}_2\text{O}_2$  was generated under X-ray irradiation of the  $\text{CeGdO}_{2-x}$  NPs' suspensions. Irradiation was conducted using an X-ray therapeutic machine RTM-15 (Mosrentgen, Moscow, Russia) in a dose of 5 Gy, at a dose rate of 1 Gy/min, 200 kV voltage, 37.5 cm focal length, and 20 mA current. To evaluate the redox activity of the  $\text{CeGdO}_{2-x}$  NPs, the concentration of hydrogen peroxide after the X-ray exposure was measured by an enhanced chemiluminescence technique, using a luminol–4-iodophenol–peroxidase system [27]. A TRIS buffer was used to maintain a constant pH (7.2). A liquid scintillation Beta-1 counter (MedApparatura, Kyiv, Ukraine), operating in a single photon counting mode (with one photomultiplier and the coincidence scheme disengaged), was used as a highly sensitive chemiluminometer. The high sensitivity of this method enabled the registration of hydrogen peroxide at a concentration of  $<1$  nM. The  $\text{H}_2\text{O}_2$  content was determined using calibration chemiluminescence plots. The concentration of hydrogen peroxide used for the calibration was determined spectrophotometrically at 240 nm, using a molar absorption coefficient of  $43.6 \text{ M}^{-1}\cdot\text{cm}^{-1}$ .

### 2.10. Statistical Data Analysis

Mean values and the standard deviation of the mean were calculated and the significance of differences between the groups was determined using the Student *t*-test.

## 3. Results

For the synthesis of the  $\text{CeGdO}_{2-x}$  nanoparticles, cerium chloride and gadolinium nitrate were used (Figure 1a). Sodium citrate was used as a biocompatible stabiliser. The results of the X-ray diffraction analysis of the  $\text{CeGdO}_{2-x}$  nanoparticles indicated their ultrasmall size and crystallinity. The X-ray diffraction pattern was characteristic of the cubic Fm3m structure of nanocrystalline ceria. According to the Scherrer formula, the crystal size of the  $\text{CeGdO}_{2-x}$  nanoparticles was 2 nm. TEM data (Figure 1b) agreed well with the X-ray

diffraction analysis, although individual nanoparticles could hardly be seen, due to the stabiliser layer. The chemical composition of the  $\text{CeGdO}_{2-x}$  nanoparticles was confirmed with an EDX analysis (Figure 1c). The hydrodynamic diameter of the nanoparticles in water was 6–7 nm (Figure 1d) and the UV spectrum possessed a peak characteristic of ceria at 340 nm (Figure 1e). Zeta potential of the  $\text{CeGdO}_{2-x}$  nanoparticles was  $-45.3$  mV (Figure 1f). We analyzed the aggregation stability of  $\text{CeGdO}_{2-x}$  nanoparticles in various medium, which confirmed their high degree of colloidal stability (Table S1).

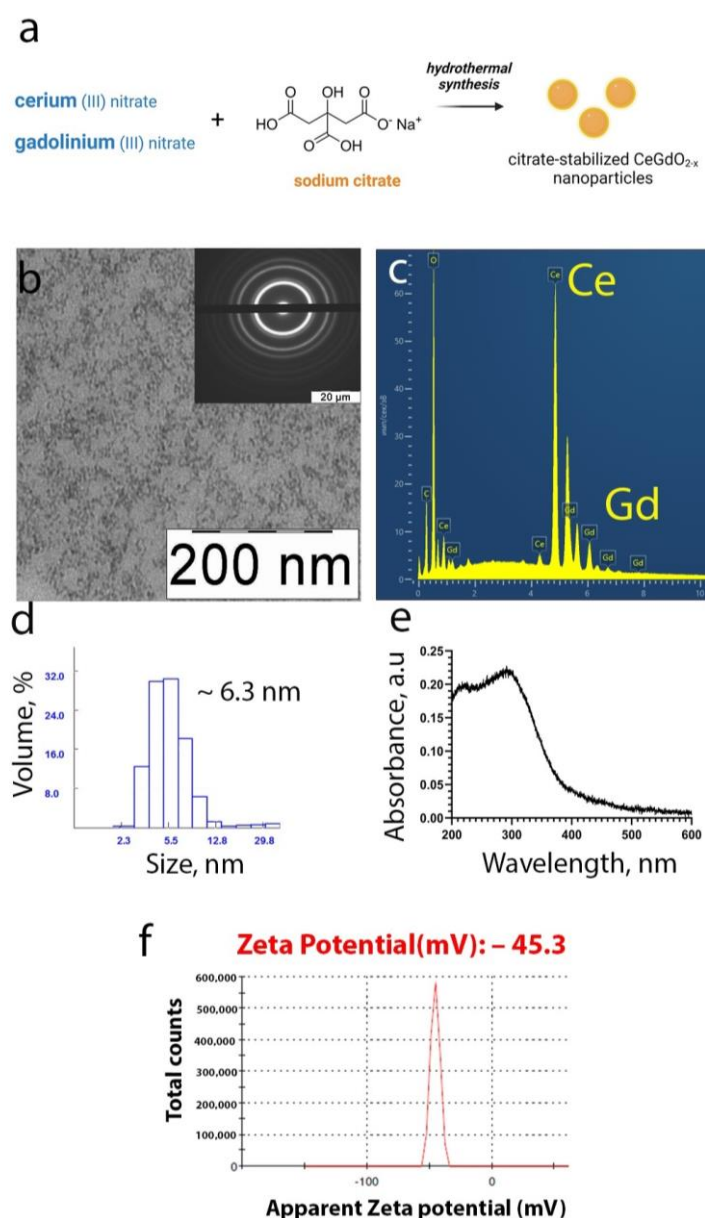


**Figure 1.** Synthesis scheme of the  $\text{CeGdO}_{2-x}$  nanoparticles (a), transmission electron microscopy (b), EDX analysis (c), dynamic light scattering in MQ water (d), UV absorbance spectrum (e) and zeta-potential (f).

The degree of crystallinity of the cerium oxide nanoparticles plays a key role in their enzyme-like properties. It was previously shown that the synthesis of cerium oxide nanoparticles under mild conditions using hydrothermal methods makes it possible to obtain nanoparticles with a low level of crystallinity and a higher content of  $\text{Ce}^{3+}$ , which ensures their high antioxidant activity. Conversely, cerium oxide nanoparticles prepared using prolonged high-temperature annealing show negligible enzyme-like properties and

are unable to protect human MSCs from oxidative stress [28]. The degree of crystallinity could also affect the biodegradability of ceria NPs. For example, Plakhova et al. have showed that the anti- and pro-oxidant activity of ceria measured at different pH levels can be related to the dissolution of cerium oxide in aqueous media [29]. Thus, the conditions for the synthesis of cerium oxide nanoparticles were chosen to achieve low toxicity and high enzyme-like activity.

Next, the redox activity of the synthesized nanoparticles was analyzed in different media to reveal their pronounced antioxidant properties (Figure 2). The properties were demonstrated for the  $\text{CeGdO}_{2-x}$  nanoparticles in aqueous solutions upon the X-ray irradiation (Figure 2a). The study showed that, at a concentration of nanoparticles of 250  $\mu\text{M}$ , the amount of the hydrogen peroxide formed was reduced by a factor of three in comparison with the control experiment. At a concentration of nanoparticles of 1 mM, the level of hydrogen peroxide in the sol after the X-ray irradiation was equal to zero (Figure 2b). These data are consistent with the authors' earlier data on the antioxidant properties of  $\text{CeO}_2$  nanoparticles, which showed that, at the concentration of  $10^{-5}$  M, they were able to effectively reduce the generation of radiation-induced hydrogen peroxide [30]. The redox properties of nanoceria enables it to work as a scavenger of reactive oxygen species (ROS) and free radicals, preventing the development of radiation-induced damage to cells, organs, and whole organisms [31–35]. It has previously been shown that nanoceria is capable of inactivating a wide range of radicals and ROSs, including the hydroxyl radical [36], nitroxyl radical [37], singlet oxygen [38], and superoxide anion radical [39]. Nanoceria is generally considered as a unique inorganic nanozyme with a wide spectrum of scavenging and anti-inflammatory activity, which makes it promising in the treatment of various diseases.

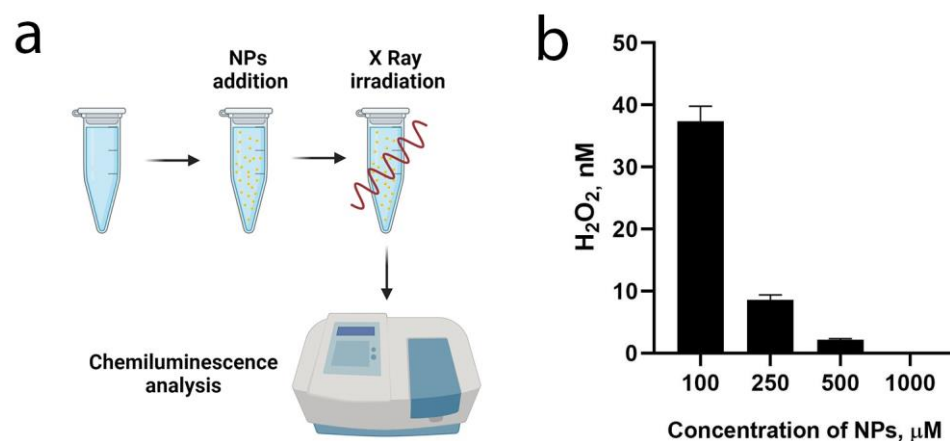


**Figure 2.** Antioxidant activity of  $\text{CeGdO}_{2-x}$  NPs under X-ray irradiation (5 Gy). Schematic representation of the experiment (a). Concentration of hydrogen peroxide after X-ray irradiation (total dose 5 Gy, 1 Gy per min) in  $\text{CeGdO}_{2-x}$  NPs colloid solution at pH 7.2 (b). The level of hydrogen peroxide was determined by the chemiluminescent method, using horseradish peroxidase.

The method of layer-by-layer adsorption of differently charged polyelectrolytes was used for the synthesis of the microcapsules, as shown in Figure 3a. The efficiency of LBL capsule formation was confirmed by zeta potential analysis after deposition of each polyelectrolyte layer (Figure S1). The integration of  $\text{CeGdO}_{2-x}$  nanoparticles into the middle layer was carried out by mixing the sol of the nanoparticles with a negatively charged polyelectrolyte (dextran sulfate). Interestingly, the integration of  $\text{CeGdO}_{2-x}$  nanoparticles in the capsules provided them a luminescent property, which was revealed using a confocal microscope (Figure 3b,c). The reason for the bright glow was not investigated since this was outside the scope of the work. The study of the microcapsules by transmission electron microscopy confirmed the effective sorption of nanoparticles, which is indicated by dark areas throughout the microcapsule (Figure 3d). The integration of nanoparticles into the structure of microcapsules was also confirmed by scanning electron microscopy,

where nanoparticle aggregates can be observed at high magnification (Figure 3e–g). Energy dispersive spectroscopy (EDX) confirmed the presence of cerium and gadolinium in the structure of the synthesized microcapsules (Figure 3i,j). The UV-visible spectrum of the synthesized microcapsules is shown in Figure 3h, which shows the peak characteristic of nanocrystalline ceria.

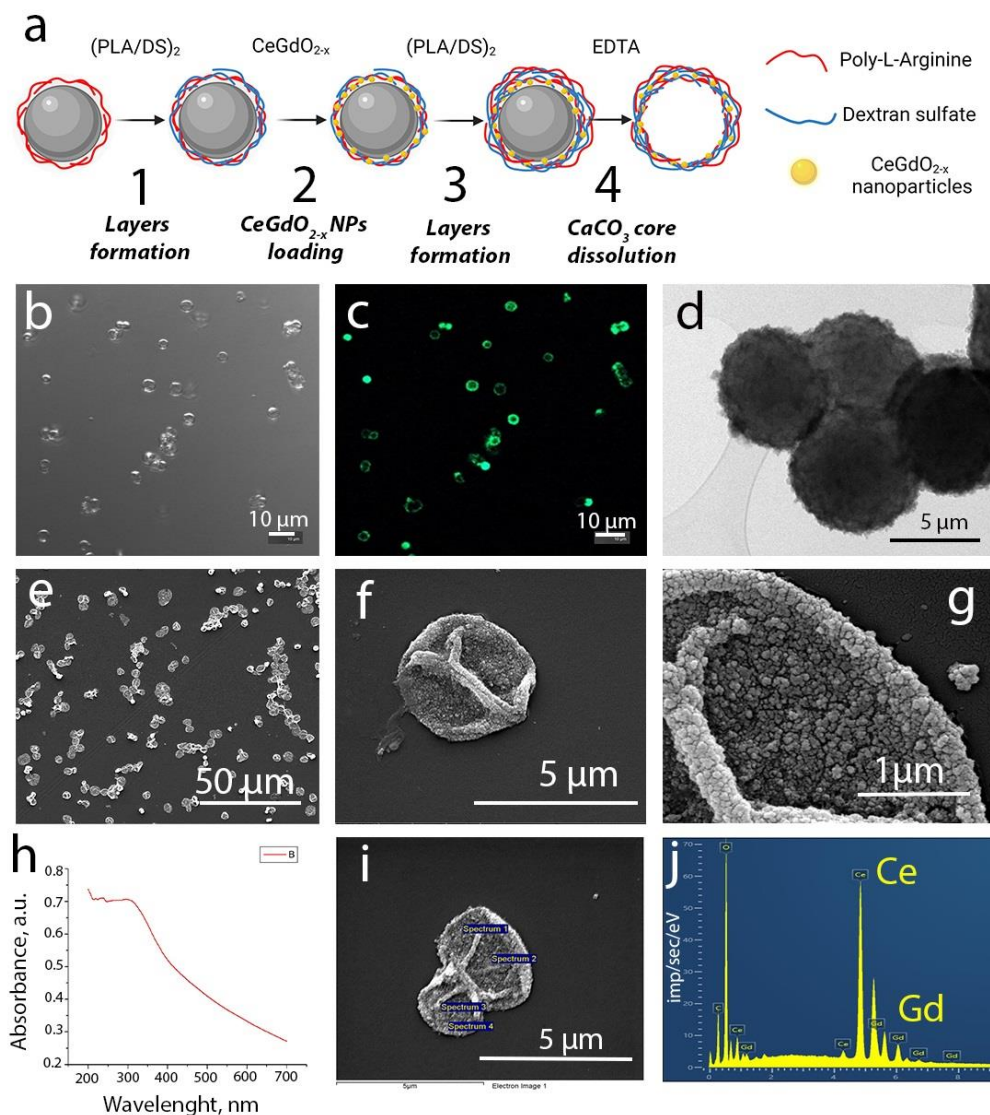


**Figure 3.** Scheme of  $\text{CeGdO}_{2-x}$  NPs-loaded microcapsules synthesis (a), LSCM (b,c), TEM (d) and SEM (e–g) images. UV-visible spectrum (h) and EDX analysis (i,j).

The polyelectrolyte microcapsules can be taken up by various types of cells, including non-phagocytic cells. The process of endocytosis of the polyelectrolyte microcapsules has been well studied, and has been demonstrated in both in vitro systems and in vivo models. Prior to this, the mechanisms of the penetration of the capsules into cells with the help of pharmacological inhibitors were studied [40]. It was shown that the main mechanism of the penetration of the capsules into human hepatocellular carcinoma HepG2 cells is endocytosis. At the same time, the deformability/stiffness of the microcapsules govern the rate of both endocytosis and exocytosis. It should be noted, however, that micron-sized capsules can be absorbed not only by phagocytic cells, but also by many others [41]. The shape of the microcapsules influences the penetration efficiency into smooth muscle cells and macrophages, through bending and faster internalization [42]. In this study, spherical capsules were used, and this shape facilitated a fairly effective uptake by cells of various

types, including human hMSCs (Figure 4). It should be noted that the loading of capsules with nanoparticles led to a change in the structure of the outer shell of the microcapsules and an increase in its roughness (Figure 3d), which provided additional sites for interaction with the cell membranes, and thus increased the absorption efficiency. It has been shown that human osteosarcoma cells (MNNG/Hos line) and human adenocarcinoma cells (MCF-7 line) also efficiently took up the hybrid microcapsules containing gadolinium-doped cerium oxide nanoparticles.

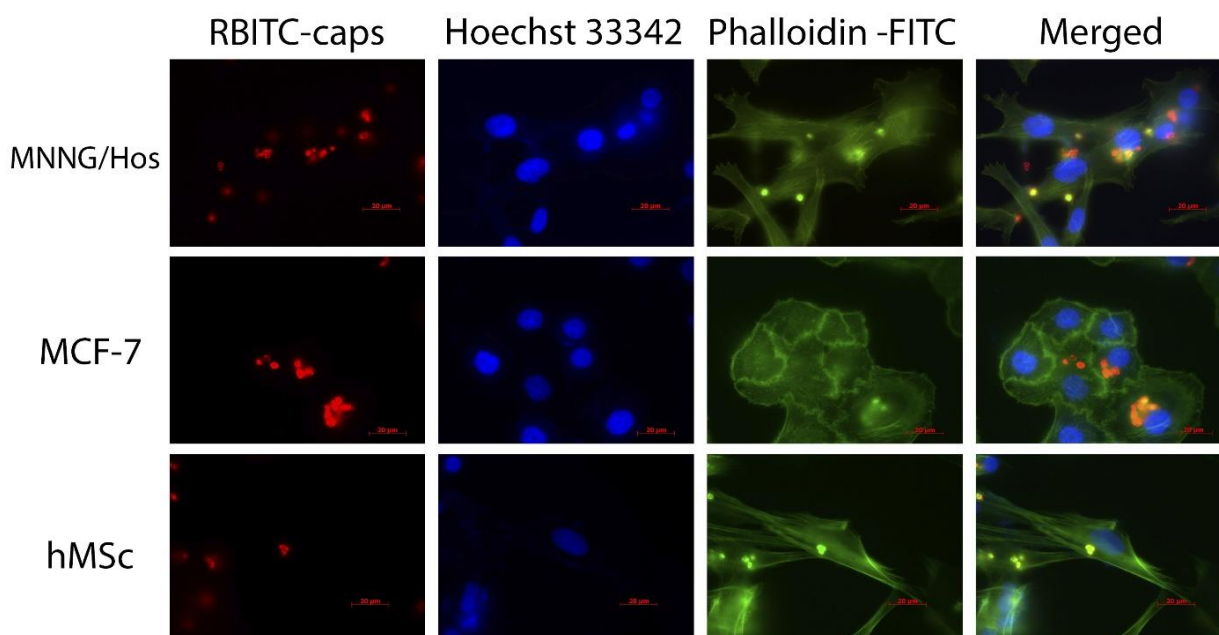


**Figure 4.** Cellular uptake of RBITC-labelled  $\text{CeGdO}_{2-x}$  NPs-loaded LbL microcapsules. Different types of cells (MNNG/Hos, MCF-7 and hMSc) were stained by phalloidin-FITC (green, actin cytoskeleton staining) and Hoechst 33,342 (blue, cell nucleus staining). Scale bar is 20  $\mu\text{m}$ .

Thus, the integration of redox-active nanoparticles into the shell of microcapsules made it possible to simultaneously deliver a much higher concentration of nanoparticles into the cells compared to a bare sol of nanoparticles.

Next, a comprehensive analysis was carried out of the cytotoxicity of the synthesized microcapsules on three types of cell cultures: human osteosarcoma MNNG/Hos cells, human adenocarcinoma MCF-7 cells, and mesenchymal stem cells isolated from human dental pulp. Two tests were used for analysis: an MTT test to analyze the level of dehydrogenase activity, and an LDH test to detect dead (lysed) cells (Figure 5). It was found that the capsules at the highest concentration (100 capsules per cell) after 24 h of co-incubation caused a significant decrease in the level of viability for all types of cell cultures studied. Further incubation (48 and 72 h) confirmed the negative effect of the microcapsules at high concentrations; the viability of the cells was reduced to 80% for human MSCs and to 84% for MNNG/Hos cells. However, low concentrations of capsules (1 or 10 capsules per cell) did not cause a statistically significant decrease in the cell viability, while a downward concentration trend was observed for all the cell types. The most sensitive to the contact with the capsules were human MSCs. At the same time, the analysis of the level of free lactate dehydrogenase (LDH assay) did not reveal statistically significant differences, which presumably indicates that the capsules affect the cells' metabolic profile and their proliferative and migratory activity, but do not cause any damage to cell membranes or cause their death even at high concentrations. Studies of the toxicity of magnetic capsules to human MSCs synthesized from poly(allyl)amine hydrochloride and poly(styrene) sulfonate were reported recently [43]. It has been shown that, at concentrations of less than 100 microcapsules per cell, they were not toxic and can be effectively internalized. It has also

been shown that hMSCs can be efficiently loaded with microcapsules without damaging the cell's structural integrity [44]. The LbL microcapsules were not shown to reduce cell viability but changed the structure of the actin cytoskeleton of cells [45]. Thus, it can be concluded that the synthesized microcapsules have a high level of biocompatibility.

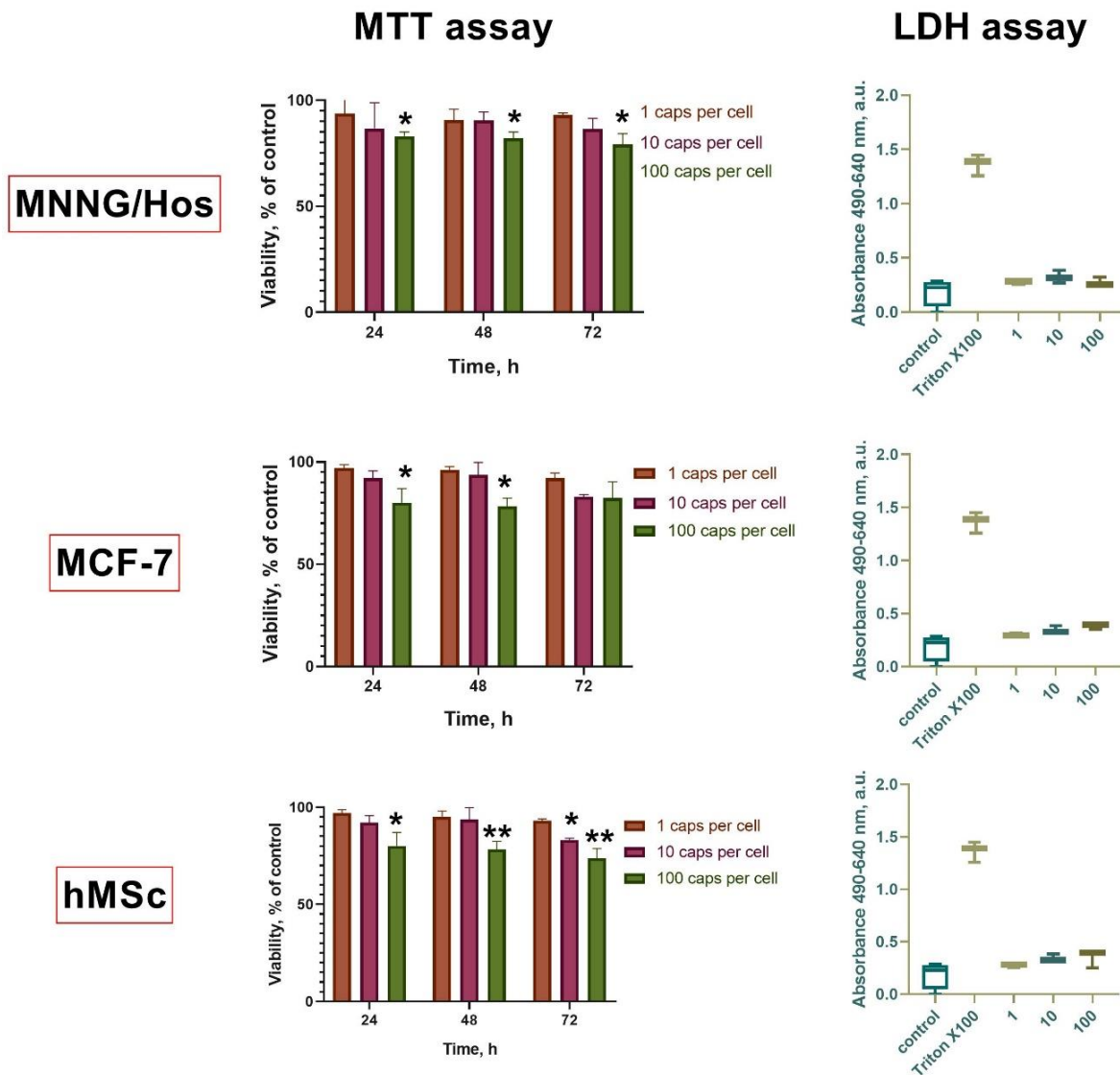


**Figure 5.** MTT assay 24, 48, and 72 h after incubation with microcapsules (1, 10 or 100 per cell), LDH assay 72 h after incubation with CeGdO<sub>2-x</sub> microcapsules (1, 10, or 100 per cell). \*  $p \leq 0.05$ , \*\*  $p \leq 0.01$ .

The next task was to find out how the integration of the nanoparticles into the structure of the capsules affects the relaxation rate in MRI measurements (Figure 6). Previously, the authors demonstrated the MRI contrast ability of dextran-stabilized gadolinium-doped cerium oxide nanoparticles [46], which amounted to  $3.6 \text{ mM} \cdot \text{s}^{-1}$ . The analysis of the relaxation rate of the synthesized LbL capsules loaded with CeGdO<sub>2-x</sub> NPs demonstrated their lower relaxation rate ( $2.75 \text{ mM} \cdot \text{s}^{-1}$ ), which could be due to the aggregation of CeGdO<sub>2-x</sub> NPs in the structure of the polyelectrolyte matrix and the low access level to water molecules (electron spins), or the possible partial loss of the nanoparticles during the multistage synthesis of the composite capsules, as previously shown [47]. At the same time, it should be noted that the relaxation rate for such CeGdO<sub>2-x</sub> loaded microcapsules is significantly inferior to commercial preparations [48]. Given that, after the internalization of such microcapsules by the cells, the loaded nanoparticles were released and distributed in the

cytoplasm, it can be assumed that the relaxation rate parameter should increase. There are different ways to incorporate gadolinium compounds into the capsules, e.g., they can be loaded into the internal compartment of the capsules. Meanwhile, the question of how to fix a gadolinium compound in the center of a capsule instead of allowing it to move freely inside a capsule still remains unresolved. The second approach is to incorporate gadolinium compounds into the capsule shell; this can be achieved by conjugating contrast agents to a polyelectrolyte, or by using nanoparticles with a high surface charge, which will bind to an oppositely charged polyelectrolyte. The latter approach was used in this study. It is very important to provide linking spacers that have good rigidity to bridge the ligand and the polymer. It is also necessary to take into account the influence of the template solvent, since the pH value of such a solvent can affect the properties of the loaded paramagnetic nanoparticles, the degree of their aggregation, and possible dissolution. Thus, the use of paramagnetic particles makes it possible to create MRI agents based on LbL capsules; however, it is necessary to ensure certain conditions for the integration of nanoparticles into the capsule structure are met, and to select conditions for the synthesis and localization of nanoparticles, which governs their MRI contrasting property.

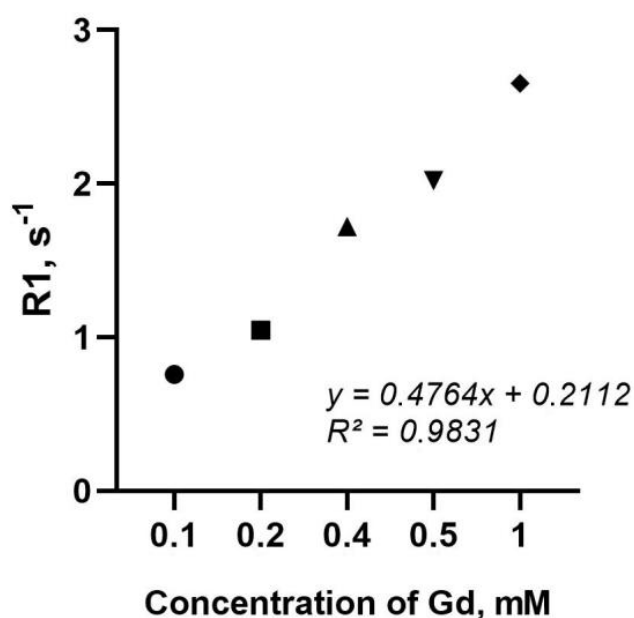


**Figure 6.**  $R_1$ -relaxation rates for  $\text{CeGdO}_{2-x}$  NPs-loaded LbL capsules at different concentrations of Gd.

#### 4. Conclusions

This paper has demonstrated the fabrication of biodegradable microcapsules with  $\text{CeGdO}_{2-x}$  NPs nanoparticles in their shell with an MRI contrasting property. The new microcapsules had a size of 3–4  $\mu\text{m}$ . A comprehensive analysis of their physicochemical properties has confirmed the effective loading of nanoparticles into the structure of the capsules. Furthermore, the synthesized capsules effectively penetrated both normal and cancer cells, being localized in the cytoplasm after the internalization. The microcapsules were not toxic at concentrations below 100 capsules per cell. The combination of MRI imaging and the redox properties of the capsules opens up possibilities for their use as theranostic agents and drug carriers with an easy to trace localization.

**Supplementary Materials:** The following supporting information can be downloaded at: <https://www.mdpi.com/article/10.3390/polym15183840/s1>, Table S1: The aggregative stability of  $\text{CeGdO}_{2-x}$  NPs via DLS study in different medium. Figure S1: Changes in zeta potential of  $\text{CeGdO}_{2-x}$  loaded capsules while layer by layer assembly. Layer 1st, 3rd, 5th: positively charge (poly-l- arginine). Layer

2nd, 4th, 6th: negatively charge (2nd and 6th dextran sulphate, 4th—citrate-stabilized CeGdO<sub>2-x</sub> NPs) applied on calcium carbonate template.

**Author Contributions:** Conceptualization, A.L.P. and V.K.I.; methodology, I.V.S.; investigation, D.D.K., N.N.C., I.V.S., E.A.M. and N.R.P.; data curation, A.L.P.; writing—original draft preparation, A.L.P., A.E.B., M.M.S. and V.K.I.; writing—review and editing, A.L.P., A.E.B. and V.K.I.; visualization, N.N.C.; supervision, A.L.P.; project administration, A.L.P.; funding acquisition, A.L.P. All authors have read and agreed to the published version of the manuscript.

**Funding:** The work was supported by the State Assignment of the Ministry of Science and Higher Education of the Russian Federation for Institute of Theoretical and Experimental Biophysics of the Russian Academy of Sciences (No. 075-01025-23-01).

**Institutional Review Board Statement:** The in vitro experiments were performed in agreement with good clinical practice and the ethical principles of the current edition of the Declaration of Helsinki, after the permission of the Ethics Committee of the Institute of Theoretical and Experimental Biophysics of the Russian Academy of Sciences (Puschino, Moscow region, Russian Federation), protocol No. 35 on 5 March 2022. Postnatal human dental pulp stem cells were extracted from the third molar tooth of a 12-year-old human donor. The tooth was removed according to the orthodontic indications of the dental clinic «Dr. MUN» (Moscow, Russia), in accordance with the ethics committee, after consent was signed by the patient's parents. All the experiments were carried out in agreement with good clinical practice and the ethical principles of the current edition of the Declaration of Helsinki.

**Informed Consent Statement:** Informed consent was obtained from all subjects involved in the study.

**Data Availability Statement:** Data is contained within the article or Supplementary Materials.

**Acknowledgments:** We express our gratitude to Shcherbakov A.B. for discussion of the experimental results.

**Conflicts of Interest:** The authors declare no conflict of interest.

## References

1. Blumfield, E.; Swenson, D.W.; Iyer, R.S.; Stanescu, A.L. Gadolinium-based contrast agents—Review of recent literature on magnetic resonance imaging signal intensity changes and tissue deposits, with emphasis on pediatric patients. *Pediatr. Radiol.* **2019**, *49*, 448–457. [[CrossRef](#)]
2. Sadowski, E.A.; Bennett, L.K.; Chan, M.R.; Wentland, A.L.; Garrett, A.L.; Garrett, R.W.; Djamali, A. Nephrogenic systemic fibrosis: Risk factors and incidence estimation. *Radiology* **2007**, *243*, 148–157. [[CrossRef](#)]
3. Swaminathan, A.S.; Horn, T.D.; Pellowski, D.; Abul-Ezz, S.; Bornhorst, J.A.; Viswamitra, S.; Shah, S.V. Nephrogenic systemic fibrosis, gadolinium, and iron mobilization. *N. Engl. J. Med.* **2007**, *357*, 720–722. [[CrossRef](#)]
4. Louis, C.; Bazzi, R.; Marquette, C.A.; Bridot, J.; Roux, S.; Ledoux, G.; Mercier, B.; Blum, L.; Perriat, P.; Tillement, O. Nanosized hybrid particles with double luminescence for biological labeling. *Chem. Mater.* **2005**, *17*, 1673–1682. [[CrossRef](#)]
5. Bridot, J.; Faure, A.; Laurent, S.; Riviere, C.; Billotey, C.; Hiba, B.; Janier, M.; Josserand, V.; Coll, J.; Elst, L.V.; et al. Hybrid gadolinium oxide nanoparticles: Multimodal contrast agents for in vivo imaging. *Am. Chem. Soc.* **2007**, *129*, 5076–5084. [[CrossRef](#)]
6. Cho, M.; Sethi, R.; Narayanan, J.S.A.; Lee, S.S.; Benoit, D.N.; Taheri, N.; Decuzzi, P.; Colvin, V.L. Gadolinium oxide nanoplates with high longitudinal relaxivity for magnetic resonance imaging. *Nanoscale* **2014**, *6*, 13637–13645. [[CrossRef](#)]
7. Das, S.; Dowding, J.M.; Klump, K.E.; McGinnis, J.F.; Self, W.; Seal, S. Cerium oxide nanoparticles: Applications and prospects in nanomedicine. *Small* **2009**, *5*, 2848–2856. [[CrossRef](#)] [[PubMed](#)]
8. Baker, C.H. Harnessing cerium oxide nanoparticles to protect normal tissue from radiation damage. *Transl. Cancer Res.* **2013**, *2*, 343–358.
9. von Montfort, C.; Alili, L.; Teuber-Hanselmann, S.; Brenneisen, P. Redox-active cerium oxide nanoparticles protect human dermal fibroblasts from PQ-induced damage. *Redox Biol.* **2015**, *4*, 1–5. [[CrossRef](#)] [[PubMed](#)]
10. Eriksson, P.; Truong, A.H.T.; Brommesson, C.; Rietz, A.; Kokil, G.R.; Boyd, R.D.; Hu, Z.; Dang, T.T.; Persson, P.O.A.; Uvdal, K. Cerium Oxide Nanoparticles with Entrapped Gadolinium for High T1 Relaxivity and ROS-Scavenging Purposes. *ACS Omega* **2022**, *7*, 21337–21345. [[CrossRef](#)] [[PubMed](#)]
11. Wason, M.S.; Colon, J.; Das, S.; Seal, S.; Turkson, J.; Zhao, J.; Baker, C.H. Sensitization of pancreatic cancer cells to radiation by cerium oxide nanoparticle-induced ROS production. *Nanomedicine* **2013**, *9*, 558–569. [[CrossRef](#)] [[PubMed](#)]
12. Ouyang, Z.; Mainali, M.K.; Sinha, N.; Strack, G.; Altundal, Y.; Hao, Y.; Winningham, T.A.; Sajo, E.; Celli, J.; Ngwa, W. Potential of using cerium oxide nanoparticles for protecting healthy tissue during accelerated partial breast irradiation (APBI). *Phys. Medica* **2016**, *32*, 631–635. [[CrossRef](#)] [[PubMed](#)]

13. Wang, C.; Blough, E.; Dai, X.; Olajide, O.; Driscoll, H.; Leidy, J.W.; July, M.; Triest, W.E.; Wu, M. Protective Effects of Cerium Oxide Nanoparticles on MC3T3-E1 Osteoblastic Cells Exposed to X-ray Irradiation. *Cell Physiol. Biochem.* **2016**, *38*, 1510–1519. [[CrossRef](#)]
14. De Cock, L.J.; De Koker, S.; De Geest, B.G.; Grooten, J.; Vervaet, C.; Remon, J.P.; Sukhorukov, G.B.; Antipina, M.N. Polymeric multilayer capsules in drug delivery. *Angew. Chem. Int. Ed. Engl.* **2010**, *49*, 6954–6973. [[CrossRef](#)]
15. Peyratout, C.S.; Dahne, L. Tailor-made polyelectrolyte microcapsules: From multilayers to smart containers. *Angew. Chem. Int. Ed. Engl.* **2004**, *43*, 3762–3783. [[CrossRef](#)] [[PubMed](#)]
16. Ai, H.; Jones, S.A.; Lvov, Y.M. Biomedical applications of electrostatic layer-by-layer nano-assembly of polymers, enzymes, and nanoparticles. *Cell Biochem. Biophys.* **2003**, *39*, 23–43. [[CrossRef](#)]
17. He, Q.; Cui, Y.; Li, J. Molecular assembly and application of biomimetic microcapsules. *Chem. Soc. Rev.* **2009**, *38*, 2292–2303. [[CrossRef](#)]
18. del Mercato, L.L.; Rivera-Gil, P.; Abbasi, A.Z.; Ochs, M.; Ganas, C.; Zins, I.; Sonnichsen, C.; Parak, W.J. LbL multilayer capsules: Recent progress and future outlook for their use in life sciences. *Nanoscale* **2010**, *2*, 458–467. [[CrossRef](#)]
19. Sukhorukov, G.B.; Mohwald, H. Multifunctional cargo systems for biotechnology. *Trends Biotechnol.* **2007**, *25*, 93–98. [[CrossRef](#)]
20. Donath, E.; Sukhorukov, G.B.; Caruso, F.; Davis, S.A.; Möhwald, H. Novel hollow polymer shells by colloid-templated assembly of polyelectrolytes. *Angew. Chem. Int. Ed. Engl.* **1998**, *37*, 2201–2205. [[CrossRef](#)]
21. Novák, L.; Miklósi, T.S.; Nyul, D.; Shi, X.; Bányai, I. Synthesis and Characterization of Carboxymethylated Polyethylenimines. *ACS Appl. Polym. Mater.* **2023**, *5*, 7208–7219. [[CrossRef](#)]
22. Ai, H.; Jones, S.A.; de Villiers, M.M.; Lvov, Y.M. Nano-encapsulation of furosemide microcrystals for controlled drug release. *J. Control. Release* **2003**, *86*, 59–68. [[CrossRef](#)]
23. Lvov, Y.; Antipov, A.; Mamedov, A.; Mohwald, H.; Sukhorukov, G.B. Urease encapsulation in nanoorganized microshells. *Nano Lett.* **2001**, *1*, 125–128. [[CrossRef](#)]
24. Dalli, J.; Norling, L.V.; Montero-Melendez, T.; Canova, D.F.; Lashin, H.; Pavlov, A.M.; Sukhorukov, G.B.; Hinds, C.J.; Perretti, M. Microparticle alpha-2-macroglobulin enhances pro-resolving responses and promotes survival in sepsis. *EMBO Mol. Med.* **2014**, *6*, 27–42. [[CrossRef](#)] [[PubMed](#)]
25. Shchukin, D.G.; Patel, A.A.; Sukhorukov, G.B.; Lvov, Y. Nanoassembly of biodegradable microcapsules for DNA encasing. *J. Am. Chem. Soc.* **2004**, *126*, 3374–3375. [[CrossRef](#)] [[PubMed](#)]
26. Popov, A.L.; Popova, N.R.; Selezneva, I.I.; Akkizov, A.Y.; Ivanov, V.K. Cerium oxide nanoparticles stimulate proliferation of primary mouse embryonic fibroblasts in vitro. *Mater. Sci. Eng. C* **2016**, *68*, 406–413. [[CrossRef](#)] [[PubMed](#)]
27. Asadullina, N.R.; Usacheva, A.M.; Smirnova, V.S.; Gudkov, S.V. Antioxidative and Radiation Modulating Properties of Guanosine-5'-Monophosphate. *Nucleosides Nucleotides Nucleic Acids* **2010**, *29*, 786–799. [[CrossRef](#)]
28. Li, F.; Yang, L.; Zou, L.; Wu, Y.; Hu, C.; He, J.; Yang, X. Decreasing Crystallinity is Beneficial to the Superoxide Dismutase-like Activity of Ceria Nanoparticles. *ChemNanoMat* **2022**, *8*, e20210046. [[CrossRef](#)]
29. Plakhova, T.V.; Romanchuk, A.Y.; Yakunin, S.N.; Dumas, T.; Demir, S.; Wang, S.; Minasian, S.G.; Shuh, D.K.; Tyliczszak, T.; Shiryaev, A.A.; et al. Solubility of Nanocrystalline Cerium Dioxide: Experimental Data and Thermodynamic Modeling. *J. Phys. Chem. C* **2016**, *120*, 22615–22626. [[CrossRef](#)]
30. Popov, A.L.; Zaichkina, S.I.; Popova, N.R.; Rozanova, O.M.; Romanchenko, S.P.; Ivanova, O.S.; Smirnov, A.A.; Mironova, E.V.; Selezneva, I.I.; Ivanov, V.K. Radioprotective effects of ultra-small citrate-stabilized cerium oxide nanoparticles. *RSC Adv.* **2016**, *6*, 106141–106149. [[CrossRef](#)]
31. Zhou, D.; Du, M.; Luo, H.; Ran, F.; Zhao, X.; Dong, Y.; Zhang, T.; Hao, J.; Li, D.; Li, J. Multifunctional mesoporous silica-cerium oxide nanozymes facilitate miR129 delivery for high-quality healing of radiation-induced skin injury. *J. Nanobiotechnol.* **2022**, *20*, 409. [[CrossRef](#)] [[PubMed](#)]
32. Kadivar, F.; Haddadi, G.; Mosleh-Shirazi, M.A.; Khajeh, F.; Tavasoli, A. Protection effect of cerium oxide nanoparticles against radiation-induced acute lung injuries in rats. *Rep. Pract. Oncol. Radiother.* **2020**, *25*, 206–211. [[CrossRef](#)]
33. Zal, Z.; Ghasemi, A.; Azizi, S.; Asgarian-Omran, H.; Montazeri, A.; Hosseinimehr, S.J. Radioprotective Effect of Cerium Oxide Nanoparticles Against Genotoxicity Induced by Ionizing Radiation on Human Lymphocytes. *Curr. Radiopharm.* **2018**, *11*, 109–115. [[CrossRef](#)]
34. Tarnuzzer, R.W.; Colon, J.; Patil, S.; Seal, S. Vacancy Engineered Ceria Nanostructures for Protection from Radiation-Induced Cellular Damage. *Nano Lett.* **2005**, *5*, 2573–2577. [[CrossRef](#)] [[PubMed](#)]
35. Colon, J.; Hsieh, N.; Ferguson, A.; Kupelian, P.; Seal, S.; Jenkins, D.W.; Baker, C.H. Cerium oxide nanoparticles protect gastrointestinal epithelium from radiation-induced damage by reduction of reactive oxygen species and upregulation of superoxide dismutase 2. *Nanomedicine* **2010**, *6*, 698–705. [[CrossRef](#)] [[PubMed](#)]
36. Lu, M.; Zhang, Y.; Wang, Y.; Jiang, M.; Yao, X. Insight into Several Factors that Affect the Conversion between Antioxidant and Oxidant Activities of Nanoceria. *ACS Appl. Mater. Interfaces* **2016**, *8*, 23580–23590. [[CrossRef](#)]
37. Dowding, J.M.; Dosani, T.; Kumar, A.; Seal, S.; Self, W.T. Cerium oxide nanoparticles scavenge nitric oxide radical ( $\cdot\text{NO}$ ). *Chem. Commun.* **2012**, *48*, 4896–4898. [[CrossRef](#)]
38. Ogawa, Y.; Kawaguchi, T.; Tanaka, M.; Hashimoto, A.; Fukui, K.; Uekawa, N.; Ozawa, T.; Kamachi, T.; Kohno, M. Quenching effect of cerium oxide nanoparticles on singlet oxygen: Validation of the potential for reaction with multiple reactive oxygen species. *J. Clin. Biochem. Nutr.* **2023**, *73*, 1–8. [[CrossRef](#)]

39. Baldim, V.; Bedioui, F.; Mignet, N.; Margail, I.; Berret, J.F. The enzyme-like catalytic activity of cerium oxide nanoparticles and its dependency on Ce<sup>3+</sup> surface area concentration. *Nanoscale* **2018**, *10*, 6971–6980. [[CrossRef](#)]
40. Yu, W.; Zhang, W.; Chen, Y.; Song, X.; Tong, W.; Mao, Z.; Gao, C. Cellular uptake of poly (allylamine hydrochloride) microcapsules with different deformability and its influence on cell functions. *J. Colloid Interface Sci.* **2016**, *465*, 149–157. [[CrossRef](#)]
41. De Koker, S.; De Geest, B.G.; Cuvelier, C.; Ferdinande, L.; Deckers, W.; Hennink, W.E.; De Smedt, S.C.; Mertens, N. In vivo Cellular Uptake, Degradation, and Biocompatibility of Polyelectrolyte Microcapsules. *Adv. Funct. Mater.* **2007**, *17*, 3754–3763. [[CrossRef](#)]
42. Li, H.; Zhang, W.; Tong, W.; Gao, C. Enhanced Cellular Uptake of Bowl-like Microcapsules. *ACS Appl. Mater. Interfaces* **2016**, *8*, 11210–11214. [[CrossRef](#)] [[PubMed](#)]
43. Lepik, K.V.; Muslimov, A.R.; Timin, A.S.; Sergeev, V.S.; Romanyuk, D.S.; Moiseev, I.S.; Popova, E.V.; Radchenko, I.L.; Vilesov, A.D.; Galibin, V.; et al. Mesenchymal Stem Cell Magnetization: Magnetic Multilayer Microcapsule Uptake, Toxicity, Impact on Functional Properties, and Perspectives for Magnetic Delivery. *Adv. Healthc. Mater.* **2016**, *5*, 3182–3190. [[CrossRef](#)] [[PubMed](#)]
44. Litvinova, L.S.; Shupletsova, V.V.; Khaziakhmatova, O.G.; Daminova, A.G.; Kudryavtseva, V.L.; Yurova, K.A.; Malashchenko, V.V.; Todosenko, N.M.; Popova, V.; Litvinov, R.I.; et al. Human Mesenchymal Stem Cells as a Carrier for a Cell-Mediated Drug Delivery. *Front. Bioeng. Biotechnol.* **2022**, *10*, 796111. [[CrossRef](#)]
45. Liu, J.; Shan, X.; Su, X.; Hu, Z.; Wang, B. Uptake of microcapsules with different stiffness and its influence on cell functions. *Colloids Surf. A Physicochem. Eng. Asp.* **2020**, *605*, 125354. [[CrossRef](#)]
46. Popov, A.; Abakumov, M.; Savintseva, I.; Ermakov, A.; Popova, N.; Ivanova, O.; Kolmanovich, D.; Baranchikov, A.; Ivanov, V. Biocompatible dextran-coated gadolinium-doped cerium oxide nanoparticles as MRI contrast agents with high T1 relaxivity and selective cytotoxicity to cancer cells. *J. Mater. Chem. B* **2021**, *9*, 6586–6599. [[CrossRef](#)]
47. German, S.V.; Bratashov, D.N.; Navolokin, N.A.; Kozlova, A.A.; Lomova, M.V.; Novoselova, M.V.; Buriylova, E.A.; Zhev, V.V.; Khlebtsov, B.N.; Bucharskaya, A.B.; et al. In vitro and in vivo MRI visualization of nanocomposite biodegradable microcapsules with tunable contrast. *Phys. Chem. Chem. Phys.* **2016**, *18*, 32238–32246. [[CrossRef](#)]
48. Rohrer, M.; Bauer, H.; Mintorovitch, J.; Requardt, M.; Weinmann, H.J. Comparison of magnetic properties of MRI contrast media solutions a different magnetic field strength. *Investig. Radiol.* **2005**, *40*, 715–724. [[CrossRef](#)]

**Disclaimer/Publisher's Note:** The statements, opinions and data contained in all publications are solely those of the individual author(s) and contributor(s) and not of MDPI and/or the editor(s). MDPI and/or the editor(s) disclaim responsibility for any injury to people or property resulting from any ideas, methods, instructions or products referred to in the content.